

Chaotic dynamics of a microswimmer in Poiseuille flow

Ricardo Chacón

Departamento de Física Aplicada, Escuela de Ingenierías Industriales, Universidad de Extremadura,
Apartado Postal 382, E-06006 Badajoz, Spain

(Received 7 June 2013; published 8 November 2013)

The chaotic dynamics of pointlike, spherical particles in cylindrical Poiseuille flow is theoretically characterized and numerically confirmed when their own intrinsic swimming velocity undergoes temporal fluctuations around an average value. Two dimensionless ratios associated with the three significant temporal scales of the problem are identified that fully determine the chaos scenario. In particular, small but finite periodic fluctuations of swimming speed result in chaotic or regular motion depending on the position and orientation of the microswimmer with respect to the flow center line. Remarkably, the spatial extension of chaotic microswimmers is found to depend crucially on the fluctuations' period and amplitude and to be highly sensitive to the Fourier spectrum of the fluctuations. This has implications for the design of artificial microswimmers.

DOI: [10.1103/PhysRevE.88.052905](https://doi.org/10.1103/PhysRevE.88.052905)

PACS number(s): 05.45.-a, 47.63.Gd, 47.61.-k, 47.63.mf

I. INTRODUCTION

The physics of microswimmers is still today a fascinating field with a long history due to the complexity arising from the coupling between their intrinsic dynamics and fluid flow, and to the ubiquity of these self-propelled entities. There are two main categories of microswimmers: microorganisms subjected to flow in diverse environments, such as pathogens in the bloodstream and sperm cells in the Fallopian tube, as well as artificial microswimmers designed for diverse applications, such as chemical sensors and drug deliverers [1–5]. A significant body of research has focused on microswimmer dynamics in confined steady flows, such as shear flow [6] and Poiseuille flow [7–10]. These studies assume a strictly constant intrinsic swimming speed. They have shown that vortices in flow reorient the swimming direction, while the swimmer's trajectories remain nonchaotic, including swinging and tumbling trajectories [10]. More complex dynamics of microswimmers that include chaos and nontrivial transport phenomena have been described for time-dependent flow fields [11,12], again assuming a strictly constant intrinsic swimming speed. While this simple assumption was sufficient to reveal the possibility of reduced transport of microswimmers in a chaotic flow due to hydrodynamic trapping [12], a more accurate description of the microswimmers' intrinsic dynamics has to consider temporal fluctuations in swimming speed. Since a microswimmer is defined as an organism or object that moves changing its shape in a *periodic* way [1], one could expect that this periodicity may cause fluctuations of the swimming speed around some average value, even when the effect of noise is negligible. Recent experiments with the green microalga *Chlamydomonas reinhardtii* have indeed demonstrated this behavior [13].

In this work, the simple case of a pointlike, spherical particle in a cylindrical Poiseuille flow is used to show that small but finite time-periodic fluctuations of the mean intrinsic swimming speed are enough to drastically change its trajectories from regular to chaotic depending on both the spectral properties of the periodic fluctuations and the position and orientation of the microswimmer with respect to the flow center line. It is demonstrated here that the extension in parameter space of this chaotic dynamics depends crucially on the relative strength of the three significant time scales

associated with the problem, but that it is robust against deviations of the microswimmer from perfect sphericity. For the sake of simplicity, it is assumed that the microswimmer stays away from bounding walls so that one can neglect steric and hydrodynamic interactions between microswimmer and walls.

II. MODEL SYSTEM

Let us consider a pointlike, spherical microswimmer that moves with an intrinsic swimming velocity $\mathbf{v}_0 = v_0 [1 + \varepsilon f(t)] \hat{\mathbf{e}}$, where $f(t)$ is a T -periodic function of unit amplitude accounting for the small fluctuations ($\varepsilon \ll 1$) around the average intrinsic speed v_0 . The equations of motion of such a microswimmer in a cylindrical channel where there exists a Poiseuille flow $\mathbf{v}_f = v_f (1 - \rho^2/R_{\text{Ch}}^2) \hat{\mathbf{z}}$ are given by [10]

$$\frac{d\mathbf{r}}{dt} = \mathbf{v}_0 + \mathbf{v}_f, \quad \frac{d\hat{\mathbf{e}}}{dt} = \frac{1}{2} \Omega_f \times \hat{\mathbf{e}}, \quad (1)$$

where \mathbf{r} and $\hat{\mathbf{e}}$ are, respectively, the position and orientation of the microswimmer, while $\Omega_f = \nabla \times \mathbf{v}_f$ is the flow vorticity, and where cylindrical coordinates (ρ, ϕ, z) and associated coordinate basis $(\hat{\rho}, \hat{\phi}, \hat{\mathbf{z}})$ are used. The microswimmer orientation $\hat{\mathbf{e}} = e_\rho \hat{\rho} + e_\phi \hat{\phi} + e_z \hat{\mathbf{z}}$ is defined by means of two angles (Fig. 1):

$$e_\rho = -\cos \Theta \sin \Psi, \quad e_\phi = \sin \Theta, \quad e_z = -\cos \Theta \cos \Psi,$$

where $\Theta \in [-\pi/2, \pi/2]$ measures the orientation in the azimuthal ϕ direction while $\Psi \in [-\pi, \pi]$ is the angle in the ρ - z plane. Since the problem presents *three* characteristic time scales ($T, t_0 \equiv R_{\text{Ch}}/v_0, t_f \equiv R_{\text{Ch}}/v_f$), it is convenient to henceforth use rescaled quantities ($\rho/R_{\text{Ch}} \rightarrow \rho \in [0, 1]$, $z/R_{\text{Ch}} \rightarrow z$, $t/t_0 \rightarrow t$) and to define the *two* essential dimensionless ratios controlling the chaos scenario: $\tau_1 \equiv t_0/T$ and $\tau_2 \equiv t_0/t_f = v_f/v_0$.

Let us first consider two-dimensional (2D) solutions of Eq. (1), i.e., $\Theta = 0$ [10], since they already capture the essence of the microswimmer's chaotic dynamics. In such a case, the trajectories of the microswimmer are restricted to two dimensions, for instance, to the x - z plane, $x \in [0, 1]$, and the translational symmetry in the z direction implies that only

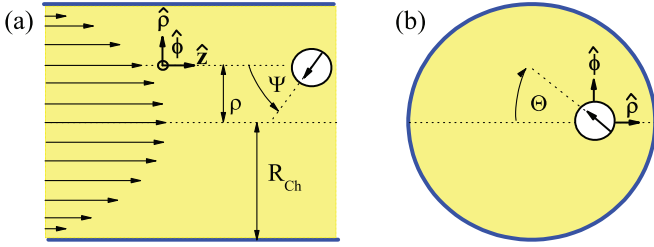


FIG. 1. (Color online) (a) Poiseuille flow profile, coordinate system and angle Ψ characterizing the projected orientation of the microswimmer onto the ρ - z plane. (b) Cross section of the channel where the angle Θ characterizes the orientation of the microswimmer in the ϕ direction.

the equations for x and Ψ are coupled:

$$\dot{x} = -[1 + \varepsilon f(t_0 t)] \sin \Psi, \quad \dot{\Psi} = \tau_2 x.$$

Eliminating x from these equations, one obtains

$$\ddot{\Psi} + \tau_2 [1 + \varepsilon f(t_0 t)] \sin \Psi = 0, \quad (2)$$

while the full 2D trajectory is obtained with the aid of the additional equation

$$\dot{z} = \tau_2(1 - x^2) - [1 + \varepsilon f(t_0 t)] \cos \Psi. \quad (3)$$

As an illustrative working model for the periodic multiharmonic fluctuation, the function

$$f(t; T, m) = N(m) \operatorname{sn} \left[\frac{4Kt}{T}; m \right] \operatorname{dn} \left[\frac{4Kt}{T}; m \right]$$

will be considered in the following. In this function, $\operatorname{sn}(\dots; m)$, $\operatorname{dn}(\dots; m)$ are Jacobian elliptic functions of parameter $m \in [0, 1]$, $K = K(m)$ is the complete elliptic integral of the first kind, and $N(m)$ is a normalization factor (see Fig. 2). When $m = 0$, one has $f(t; T, m = 0) = \sin(2\pi t/T)$, while for the limiting value $m = 1$ the fluctuation vanishes. Note that the

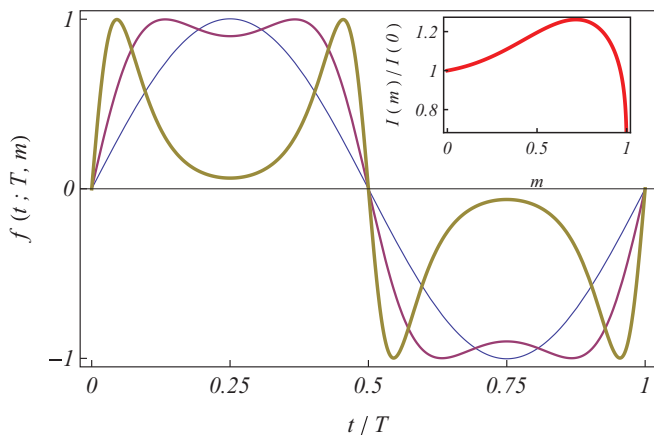


FIG. 2. (Color online) Plots of the function $f(t; T, m) = N(m) \operatorname{sn}[4K(m)t/T; m] \operatorname{dn}[4K(m)t/T; m]$ vs t , in which $N(m) \equiv 1/(a + b/[1 + \exp\{(m - c)/d\}])$ is a normalization function, with $a \equiv 0.43932, b \equiv 0.69796, c \equiv 0.3727, d \equiv 0.26883$, for three values of the elliptic parameter: $m = 0$ (thin line), $m = 0.717 \approx m_{\max}^{\text{impulse}}$ (medium line), and $m = 0.999$ (thick line). Inset: Plot of the fluctuation's impulse per half period I vs m , which presents a single maximum at $m = m_{\max}^{\text{impulse}} \approx 0.717$.

fluctuation's impulse per half period,

$$I(m) = \frac{2}{T} \int_0^{T/2} f(t; T, m) dt = \frac{N(m)}{K(m)},$$

presents a single maximum at $m = m_{\max}^{\text{impulse}} \approx 0.717$ (see Fig. 2, inset). Since Eq. (2) represents a *parametrically excited* pendulum, its phase space is three-dimensional (3D), and there always exists Hamiltonian chaos around the unperturbed separatrix in a Poincaré section [$\dot{\Psi}(t_n)$ vs $\Psi(t_n)$, $t_n = nT + t_0$, $n = 1, \dots$] for arbitrarily small but finite amplitude ε . Additionally, islands of regular elliptic regions and (stable) fixed points, which are associated respectively with quasiperiodic and periodic orbits in phase space, as well as higher-order island chains complete the picture in the Poincaré section [14]. Given Eq. (3), this means that 2D and 3D microswimmer's trajectories may be periodic, quasiperiodic, or chaotic depending on their position and orientation in the channel and the values of the parameters $\varepsilon, m, \tau_1, \tau_2$. An estimate of the width, Δ , of the chaotic layer around the unperturbed separatrix can be obtained by using Melnikov's method [14–16] (see the Appendix). Thus, using the Fourier expansion of $\operatorname{sn}(\dots; m) \operatorname{dn}(\dots; m)$, and after some simple algebraic manipulation, one may write the Melnikov function (MF) corresponding to the equivalent perturbed pendulum of Eq. (2) as

$$\begin{aligned} M^\pm(t') &= -2\varepsilon \sum_{n=0}^{\infty} a_n b_n \cos \left[\left(n + \frac{1}{2} \right) 4\pi \tau_1 t' \right], \\ a_n &= a_n(m) \equiv \frac{\pi^3 N(m) (n + \frac{1}{2})}{K^2(m) \sqrt{m} \cosh \left[\frac{(n + \frac{1}{2}) \pi K(1-m)}{K(m)} \right]}, \\ b_n &= b_n(\tau_1, \tau_2) \equiv \frac{(n + \frac{1}{2})^2 (4\pi \tau_1)^2}{\sinh \left[(n + \frac{1}{2}) 2\pi^2 \tau_1 / \sqrt{\tau_2} \right]}, \end{aligned} \quad (4)$$

where the positive (negative) sign refers to the top (bottom) homoclinic orbit of the underlying conservative pendulum:

$$\begin{aligned} \Psi_0(t) &= \pm 2 \arctan[\sinh(\sqrt{\tau_2} t)], \\ \dot{\Psi}_0(t) &= \pm 2\sqrt{\tau_2} \operatorname{sech}(\sqrt{\tau_2} t). \end{aligned}$$

As noted in the Appendix, the simple zeros of the MF imply transversal intersections of stable and unstable manifolds, giving rise to Smale horseshoes and hence hyperbolic invariant sets [15]. Thus, a homoclinic bifurcation always occurs in the present case, and an estimate of the width [16] of the subsequent chaotic separatrix layer in the aforementioned Poincaré section [cf. Eq. (A3)] is found to be

$$\begin{aligned} \Delta &= \Delta(\varepsilon, \tau_1, \tau_2, m) = \frac{|\max_{t'} M^\pm(t')|}{2\sqrt{\tau_2}} \\ &= \frac{\varepsilon}{\sqrt{\tau_2}} \sum_{n=0}^{\infty} a_n(m) b_n(\tau_1, \tau_2). \end{aligned} \quad (5)$$

The width function $\Delta(\varepsilon, \tau_1, \tau_2, m)$ provides an estimate of the width in energy of the chaotic separatrix layer since the equivalent perturbed pendulum (2) comes from the perturbed Hamiltonian $H = H_0 + \varepsilon H_1$, where

$H_0 \equiv \frac{1}{2}\dot{\Psi}^2 - \tau_2 \cos \Psi$ and $H_1 \equiv -\tau_2 f(t_0 t) \cos \Psi$. Next, the robustness of the prediction of Eq. (5) against small deviations from exact sphericity may be determined by considering the dynamics of an elongated spheroidal microswimmer with aspect ratio γ and associated geometry factor $G = (\gamma^2 - 1)/(\gamma^2 + 1) \in [0, 1]$, such that the case of exact sphericity is recovered for $\gamma = 1$ (i.e., $G = 0$) while one has $0 < G \ll 1$ for slightly elongated microswimmers. For any G , Eq. (2) is generalized to the form [17]

$$\begin{aligned}\dot{\Psi} &= \tau_2 x [1 - G \cos(2\Psi)], \\ \dot{x} &= -[1 + \varepsilon f(t_0 t)] \sin \Psi.\end{aligned}\quad (6)$$

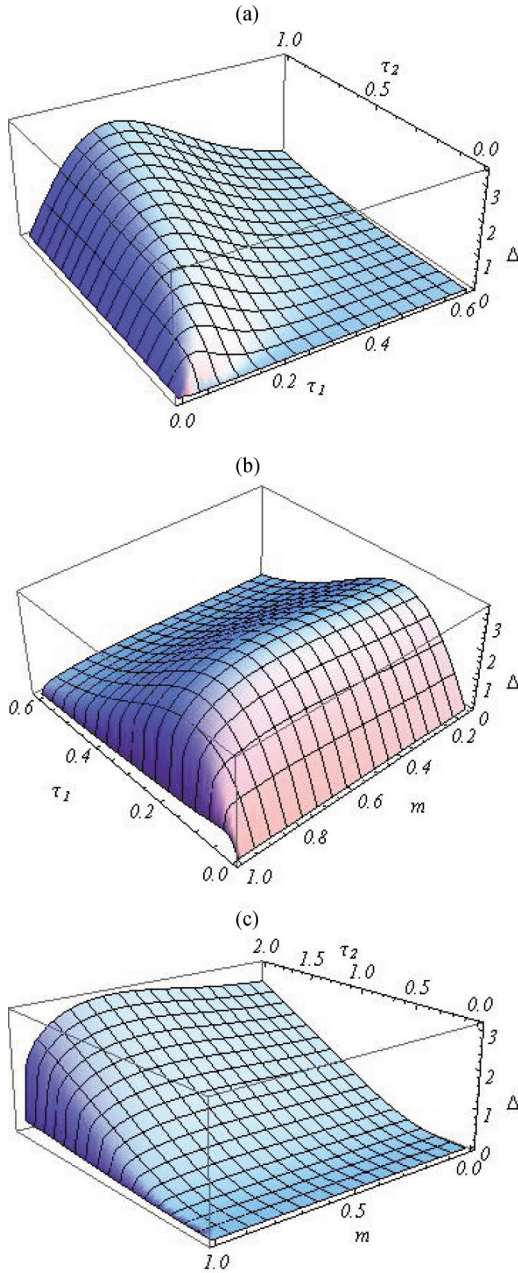


FIG. 3. (Color online) Width of the chaotic separatrix layer Δ [cf. Eq. (5) with $\varepsilon = 1$] vs (a) τ_1 and τ_2 for $m = 0$, (b) τ_1 and m for $\tau_2 = 1$, and (c) τ_2 and m for $\tau_1 = 1/2$.

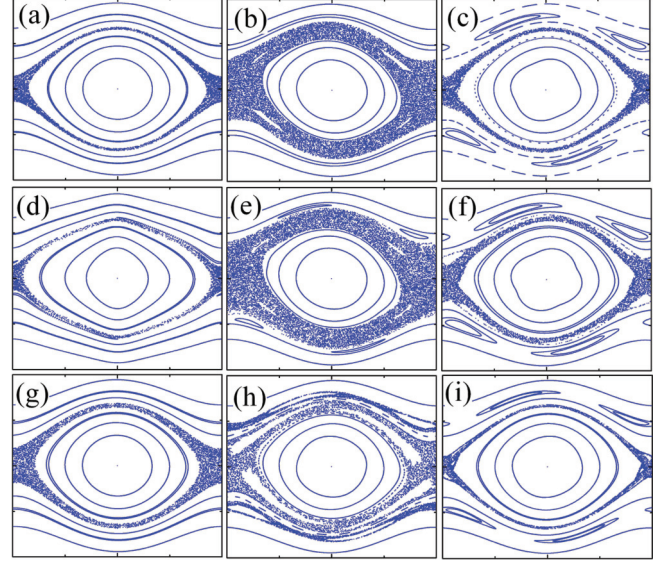


FIG. 4. (Color online) Poincaré maps of Eq. (6), $x(t_n) \in [-1, 1]$ vs $\Psi(t_n) \in [-\pi, \pi]$ associated with the section $t_n = nT$, $n = 1, \dots, 1500$, for $\tau_2 = 1$ and nine sets of the remaining parameters $(\varepsilon, m, G, \tau_1)$: (a) $(0.1, 0, 0, 0.05)$, (b) $(0.1, 0, 0, \tau_{1, \max})$, (c) $(0.1, 0, 0, 0.6)$, (d) $(0.1, 0, 0.5, 0.05)$, (e) $(0.1, m_{\max}, 0, \tau_{1, \max})$, (f) $(0.1, m_{\max}, 0, 0.6)$, (g) $(0.2, 0, 0, 0.05)$, (h) $(0.1, 0.999, 0, \tau_{1, \max})$, and (i) $(0.1, 0.999, 0, 0.6)$. The same initial conditions were used in all the versions, $\tau_{1, \max} \equiv 0.194$, and $m_{\max} \equiv 0.655$.

Thus, after assuming $0 < \tau_2 G \ll 1$, the MF corresponding to the equivalent perturbed pendulum (6) is given by Eq. (4) minus the integral

$$\tau_2 G \int_{-\infty}^{\infty} \dot{\Psi}_0(t) \sin \Psi_0(t) \cos[2\Psi_0(t)] dt,$$

which is *zero* due to its integrand being an odd function. After a careful analysis of the above results, the following remarks may now be in order (see Figs. 3 and 4).

First, an upstream, $\Psi \approx 0$ (downstream, $\Psi \approx \pi$), oriented microswimmer presents regular (chaotic) motion when it is sufficiently near the center line of the flow depending on the parameter values, and hence on the chaotic layer width, as expected from the stabilizing (destabilizing) effects of the flow vorticity. Such a regular (quasiperiodic or periodic) motion of the upstream oriented microswimmer is upstream motion when the ratio between the maximum flow speed and the average intrinsic swimming speed (τ_2) is sufficiently small [cf. Eq. (3)]. However, when the upstream-oriented microswimmer's direction departs sufficiently from the center line such that the microswimmer is inside the chaotic layer, it may move chaotically upstream ($\dot{z} < 0$), downstream ($\dot{z} > 0$), or mixed up- and down-stream depending on its distance x to the center line and the values of the amplitude ε and the ratio between the maximum flow speed and the average intrinsic swimming speed (τ_2) [cf. Eq. (3)]. Also, a downstream-oriented microswimmer presents regular (quasiperiodic or periodic) motion when it is sufficiently far from the center line of the flow depending on the parameter values, and hence again on the chaotic layer width.

Second, for τ_2 and ε constant, the width Δ presents a single maximum at $(\tau_1, m) = (\tau_{1, \max}, m_{\max})$ with $\tau_{1, \max} = \tau_{1, \max}(\tau_2)$

such that $\Delta(\varepsilon, \tau_{1, \max}, \tau_2, m_{\max})$ increases as the ratio between the maximum flow speed and the average intrinsic swimming speed (τ_2) or the amplitude ε increase [see Figs. 3(a) and 3(b), and compare Figs. 4(a), 4(b), 4(c), and 4(e)]. Note that both $\tau_{1, \max}$ and Δ increase as τ_2 increases, i.e., when the ratio between the maximum flow speed and the average intrinsic swimming speed is ever larger, irrespective of the values of ε and m [see Figs. 3(a) and 3(c)]. However, since $x = \dot{\Psi}/\tau_2$ and $b_n \sim \sqrt{\tau_2}$ as $\tau_2 \rightarrow \infty$ [cf. Eq. (4)], one obtains $\Delta \rightarrow \text{const}$ as $\tau_2 \rightarrow \infty$ in a Poincaré section $\dot{\Psi}(t_n)$ vs $\Psi(t_n)$ while $\Delta \rightarrow 0$ in a Poincaré section $x(t_n)$ vs $\Psi(t_n)$. In the other limit, $\tau_2 \rightarrow 0$ (i.e., when the ratio between the maximum flow speed and the average intrinsic swimming decreases more and more), one obtains $b_n \sim e^{-C/\sqrt{\tau_2}}$ [$C \equiv C(n, \tau_1)$, cf. Eq. (4)] and hence $\Delta \rightarrow 0$ in both kinds of Poincaré sections. Thus, chaotic behavior of microswimmers is not expected in the limits $\tau_2 \rightarrow 0, \infty$, i.e., when the maximum flow speed is much higher or much lesser than the average intrinsic swimming speed, which needs to be taken into account in designing artificial microswimmers to have regular swimming [1,18].

Third, the width Δ presents its maximum at a *single* value of the elliptic parameter $m = m_{\max} \simeq 0.655$, which *does not* depend on the remaining parameters $\varepsilon, \tau_1, \tau_2$. This means that such a value is a consequence of the Fourier spectrum of the periodic fluctuation. Specifically, m_{\max} is significantly near $m_{\max}^{\text{impulse}} \simeq 0.717$, i.e., the m value that yields *maximum* impulse per half period [compare Figs. 4(c), 4(f), and 4(i)]. Importantly, the presence of many non-negligible subharmonics in the spectrum (such as for $m \lesssim 1$) leads to richer behavior than that found in the case of a single harmonic ($m = 0$), as in the example of Fig. 4(h) where two secondary chaotic layers can be appreciated [compare Figs. 4(b) and 4(h)]. Again, this property may be useful in designing artificial microswimmers. One can understand the coincidence between m_{\max} and $m_{\max}^{\text{impulse}}$ by analyzing the variation of the pendulum's energy. Indeed, note that Eq. (2) can be put into the form

$$\frac{dE}{dt} = -\tau_2 \varepsilon f(t_0 t) \dot{\Psi} \sin \Psi, \quad (7)$$

where $E(t) \equiv \frac{1}{2} \dot{\Psi}^2(t) + U[\Psi(t)]$ [$U(\Psi) \equiv -\tau_2 \cos \Psi$] is the energy function and $f(t_0 t)$ is a Υ -periodic function with $\Upsilon \equiv T/t_0 \equiv 1/\tau_1$. Integration of Eq. (7) over *any* interval $[n\Upsilon, n\Upsilon + \Upsilon/2], n = 0, 1, 2, \dots$, yields

$$E(n\Upsilon + \Upsilon/2) - E(n\Upsilon) = -\tau_2 \varepsilon \int_{n\Upsilon}^{n\Upsilon + \Upsilon/2} f(t_0 t) \dot{\Psi} \sin \Psi dt. \quad (8)$$

Now, for the present choice $f(t_0 t) = N(m) \text{sn}[4Kt/\Upsilon; m] \text{dn}[4Kt/\Upsilon; m]$, if one considers fixing the parameters $(\varepsilon, \tau_1, \tau_2)$ for the equivalent perturbed pendulum to lie at a periodic orbit inside the initial well (near the underlying separatrix as required by Melnikov's method) at $m = 0$, the application of the first mean value theorem [19] to the integral on the r.h.s. of Eq. (8) gives

$$E(n\Upsilon + \Upsilon/2) - E(n\Upsilon) = -\tau_2 \varepsilon \Upsilon \dot{\Psi}(t^*) \sin \Psi(t^*) I(m)/2, \quad (9)$$

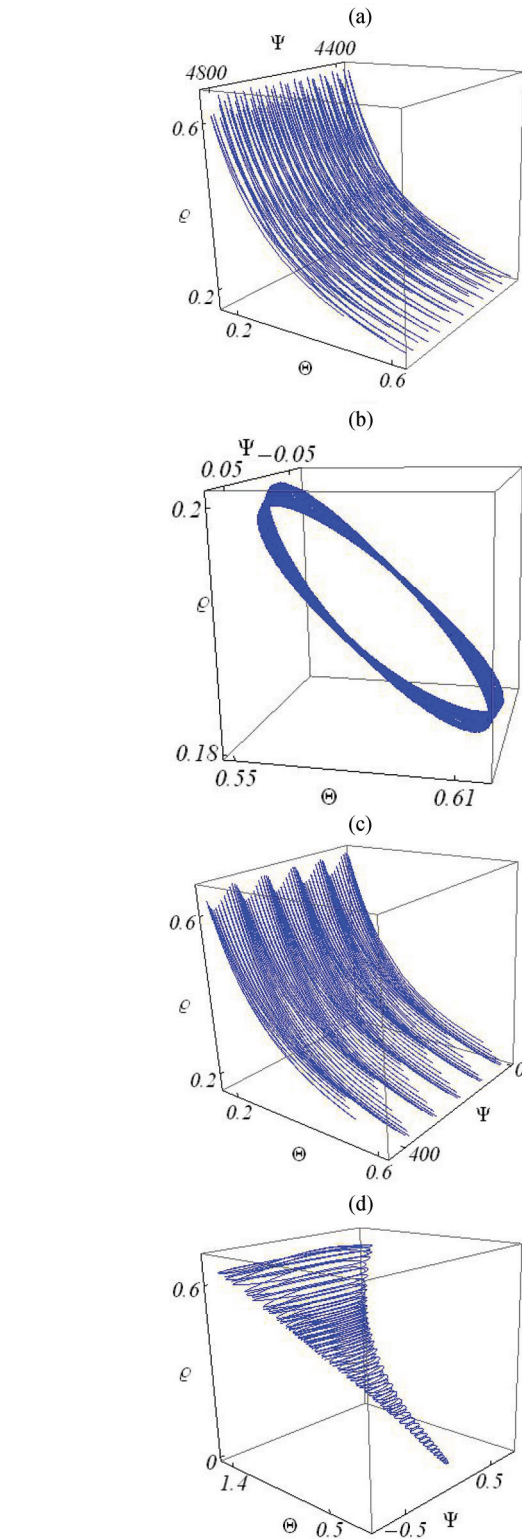


FIG. 5. (Color online) Typical trajectories for chaotic (a), (d), quasiperiodic (b), and periodic (c) motion in the ρ - Ψ - Θ phase space [cf. Eq. (10)] for $\tau_2 = 10, m = 0, \rho(t=0) = 0.2, \Theta(t=0) = 0.55$. (a) $\Psi(t=0) = \pi, \varepsilon = 0.15, \tau_1 = 0.2$. (b) $\Psi(t=0) = 0, \varepsilon = 0.15, \tau_1 = 0.2$. (c) $\Psi(t=0) = \pi, \varepsilon = 0.15, \tau_1 = 0.05$. (d) $\Psi(t=0) = 0, \varepsilon = 0.9, \tau_1 = 0.95$.

where $t^* \in [n\Upsilon, n\Upsilon + \Upsilon/2]$. Since the initial state is a steady (periodic) state, t^* will depend solely on the function $f(t_0 t)$

but not on n . In this situation, one increases m while holding constant the remaining parameters. For values $m > 0$ such that the state of the equivalent perturbed pendulum is still a periodic orbit inside the initial well (which will be necessarily near the initial periodic orbit in the phase space), one expects that $\dot{\Psi}(t^*) \sin \Psi(t^*)$ will maintain approximately its initial value (at $m = 0$) while the fluctuation's impulse per half period $I(m) \equiv N(m)/K(m)$ will rise from its initial value. This means that, in *some* case depending upon the remaining parameters and the sign of $\dot{\Psi}(t^*) \sin \Psi(t^*)$, the energy increment $\Delta E \equiv E(n\Upsilon + \Upsilon/2) - E(n\Upsilon)$ could be enough to surpass the threshold escape energy, i.e., the threshold oscillation amplitude to allow escape from the initial potential well and hence to reach the chaotic separatrix layer. Clearly the probability of this event is maximal at $m = m_{\max}^{\text{impulse}}$ where $I(m)$ presents an absolute maximum, which explains that $m_{\max} \simeq m_{\max}^{\text{impulse}}$. For fixed ε and τ_2 , since the fluctuation's impulse over a half period $\Upsilon I(m)/2$ depends on both the elliptic parameter and the period, its critical value yielding the aforementioned escape event can in some case be reached at $m \neq m_{\max}^{\text{impulse}}$ provided that Υ is sufficiently large.

And fourth, the prediction of Eq. (5) is expected to hold, at least for slightly elongated microswimmers [20] [compare Figs. 4(a) and 4(d)], while the width Δ is proportional to the fluctuation amplitude ε [compare Figs. 4(a) and 4(g)].

When $\Theta \neq 0$, Eq. (1) gives rise to the equations

$$\begin{aligned}\dot{\rho} &= -[1 + \varepsilon f(t_0 t)] \cos \Theta \sin \Psi, \\ \dot{\Psi} &= \tau_2 \rho - \sin \Theta \tan \Theta \cos \Psi / \rho, \\ \dot{\Theta} &= \sin \Theta \sin \Psi / \rho,\end{aligned}\quad (10)$$

which do not depend on ϕ and z because of the rotational symmetry about the channel axis and the translational symmetry in the z direction, respectively. The temporal dependence of the microswimmer speed breaks the two constants of motion existing when $\varepsilon = 0$ [10], so that chaotic 3D trajectories are expected over finite regions in parameter space. Unfortunately, the mathematical complexity of Eq. (10) prevents one from obtaining analytical estimates of the chaotic regions in parameter space as was possible in the case $\Theta = 0$. Numerical experiments confirmed that the main features of the above 2D chaos scenario hold in the general case (10). Figure 5 shows some illustrative examples [21].

III. CONCLUSIONS

In summary, it has been demonstrated that periodic fluctuations of a microswimmer's swimming speed in a cylindrical Poiseuille flow give rise to dynamics of great complexity, including chaotic, quasiperiodic, and periodic motions. Two dimensionless ratios associated with the three significant temporal scales of the problem were identified that fully determine the chaos scenario. Analytical estimates were obtained characterizing the dependence of the extension of the chaos on the amplitude, period, and Fourier spectrum of the fluctuations, thus providing information that may be useful in designing and optimizing artificial microswimmers. The chaos scenario discussed in this work should be accessible in experiments with

spherical artificial microswimmers with different locomotion mechanisms [22] in channels under Poiseuille flow.

Finally, the results suggest that finely tuned upstream-oriented (downstream-oriented) swimming near (far from) the center of the flow may be an efficient evolutionary strategy to preserve regular swimming of self-propelled microorganisms in laminar flows. Remarkably, this is *exactly* the collective behavior of the microalga *C. reinhardtii* when swimming upstream (downstream) toward a light (phototaxis) [23]. The phototaxis property describes the regular orientation of certain microorganisms toward a light source. For typical parameter values considered in Refs. [23] ($v_f \sim 40$ mm/s, $v_0 \sim 50$ μ m/s, $R_{\text{Ch}} \sim 0.5$ mm) and [13] ($T \sim 19$ ms), one obtains $\tau_1 \sim 526$, $\tau_2 \sim 800$, and hence $\Delta/\varepsilon \sim 10^{-73}$; i.e., chaotic behavior is not expected [cf. second remark and Eq. (5)]. One can conjecture thus the existence of a link between phototaxis and required regular swimming, which deserves further exploration in the light of the complex dynamics of this microalga [24].

ACKNOWLEDGMENTS

The author acknowledges useful discussions with A. M. Gañán-Calvo. This research was partly supported by the Ministerio de Ciencia e Innovación (MICINN, Spain) through project FIS2012-34902, and by the Junta de Extremadura (JEx, Spain) through project GR10045.

APPENDIX: MELNIKOV'S METHOD

This Appendix briefly describes Melnikov's method for the simple case of a perturbed integrable Hamiltonian system with one degree of freedom. Consider the system

$$\dot{\mathbf{x}}_t = h_0(\mathbf{x}) + \varepsilon h_1(\mathbf{x}, t), \quad \mathbf{x} = (x_1, x_2), \quad (\text{A1})$$

where the unperturbed system ($\varepsilon = 0$) is an integrable Hamiltonian system which possesses a hyperbolic fixed point X_0 and a separatrix orbit $x_0(t)$ such that $\lim_{t \rightarrow \pm\infty} x_0(t) = X_0$ while the stable and unstable manifolds $x^s(t), x^u(t)$ are smoothly joined. Generally, the perturbation term h_1 can introduce dissipation and nonautonomous excitation, with h_1 being T periodic in time. For $\varepsilon \neq 0$, the perturbed stable and unstable manifolds no longer join smoothly such that, if the ratio of dissipation and excitation is sufficiently small, the stable and unstable manifolds will intersect transversally, creating a homoclinic point. This process is called a homoclinic bifurcation and indicates the onset of chaotic instabilities. To check when a transverse crossing occurs, Melnikov introduced a function $M(t')$ (now known as the Melnikov function) which measures the distance between the perturbed stable and unstable manifolds in the Poincaré section:

$$M(t') \equiv \int_{-\infty}^{\infty} h_0(x_0(t - t')) \wedge h_1(x_0(t - t'), t) dt, \quad (\text{A2})$$

where \wedge is the wedge operator ($\mathbf{x} \wedge \mathbf{y} = x_1 y_2 - x_2 y_1$). If the Melnikov function presents a simple zero, the manifolds intersect transversally and chaotic instabilities result. When h_1 is a Hamiltonian perturbation, this leads to the appearance of an unstable layer, meaning the possibility of persistent chaotic motion, along the separatrix of the unperturbed system. The width Δ of this chaotic separatrix layer can be estimated from

the Melnikov function as

$$\Delta = \left| \frac{\max_{t'} M(t')}{|h_0[x_0(0)]|} \right| + O(\varepsilon^2). \quad (\text{A3})$$

See Refs. [14–16] for more details about Melnikov's method.

-
- [1] E. Lauga and T. R. Powers, *Rep. Prog. Phys.* **72**, 096601 (2009).
- [2] T. J. Pedley and J. O. Kessler, *Annu. Rev. Fluid Mech.* **24**, 313 (1992).
- [3] T. Vicsek, A. Czirok, E. Ben-Jacob, I. Cohen, and O. Shochet, *Phys. Rev. Lett.* **75**, 1226 (1995).
- [4] C. Dombrowski, L. Cisneros, S. Chatkaew, R. E. Goldstein, and J. O. Kessler, *Phys. Rev. Lett.* **93**, 098103 (2004).
- [5] J. P. Hernandez-Ortiz, C. G. Stoltz, and M. D. Graham, *Phys. Rev. Lett.* **95**, 204501 (2005).
- [6] B. ten Hagen, R. Wittkowski, and H. Löwen, *Phys. Rev. E* **84**, 031105 (2011).
- [7] J. Hill, O. Kalkanci, J. L. McMurtry, and H. Koser, *Phys. Rev. Lett.* **98**, 068101 (2007).
- [8] G. Zilman, J. Novak, and Y. Benayahu, *Mar. Biol.* **154**, 1 (2008).
- [9] R. W. Nash, R. Adhikari, J. Tailleur, and M. E. Cates, *Phys. Rev. Lett.* **104**, 258101 (2010).
- [10] A. Zöttl and H. Stark, *Phys. Rev. Lett.* **108**, 218104 (2012).
- [11] C. Torney and Z. Neufeld, *Phys. Rev. Lett.* **99**, 078101 (2007).
- [12] N. Khurana, J. Blawdziewicz, and N. T. Ouellette, *Phys. Rev. Lett.* **106**, 198104 (2011).
- [13] J. S. Guasto, K. A. Johnson, and J. P. Gollub, *Phys. Rev. Lett.* **105**, 168102 (2010); K. Drescher, R. E. Goldstein, N. Michel, M. Polin, and I. Tuval, *ibid.* **105**, 168101 (2010).
- [14] A. J. Lichtenberg and M. A. Lieberman, *Regular and Chaotic Motion* (Springer-Verlag, New York, 1993).
- [15] J. Guckenheimer and P. Holmes, *Nonlinear Oscillations, Dynamical Systems, and Bifurcations of Vector Fields* (Springer-Verlag, New York, 1983).
- [16] S. Wiggins, *Chaotic Transport in Dynamical Systems* (Springer, New York, 1992).
- [17] The case $\varepsilon = 0$ was studied in A. Zöttl and H. Stark, *Eur. Phys. J. E* **36**, 4 (2013).
- [18] R. Dreyfus *et al.*, *Nature (London)* **437**, 862 (2005).
- [19] I. Gradshteyn and I. Ryzhik, *Table of Integrals, Series and Products* (Academic, New York, 1994), p. 1097.
- [20] This is not so surprising since Eq. (6) with $\varepsilon = 0$ is integrable and has a separatrix for any value of G with the same symmetry properties than that of the limiting case $G = 0$ (cf. Ref. [17]).
- [21] An exhaustive study of chaotic solutions of Eq. (10) is beyond the scope of the present work. Further details will be given elsewhere.
- [22] See, e.g., J. R. Howse, R. A. L. Jones, A. J. Ryan, T. Gough, R. Vafabakhsh, and R. Golestanian, *Phys. Rev. Lett.* **99**, 048102 (2007); J. Palacci, C. Cottin-Bizonne, C. Ybert, and L. Bocquet, *ibid.* **105**, 088304 (2010); H.-R. Jiang, N. Yoshinaga, and M. Sano, *ibid.* **105**, 268302 (2010).
- [23] X. Garcia, S. Rafai, and P. Peyla, *Phys. Rev. Lett.* **110**, 138106 (2013).
- [24] M. Garcia, S. Berti, P. Peyla, and S. Rafai, *Phys. Rev. E* **83**, 035301(R) (2011).